Published by :
http://www.ijert.org

International Journal of Engineering Research & Technology (IJERT)
ISSN: 2278-0181
Vol. 7 Issue 08, August-2018

Flow through Sinusoidal Obstructions in a Channel – Obstructions on the Same Side of the Channel

B.H.L. Gowda, B.K.Srinivas, S.R.Kiranbasil, S.Anugrah, Kiran Wilson and A.A.Lone
Department of Mechanical Engineering,
BTL Institute of Technology, Bangalore-560099

Abstract **- This paper presents flow visualization results for sinusoidal constrictions in a two-dimensional channel. The constrictions are arranged on the same side of the channel in tandem arrangement. The relative size of the obstructions and the spacing between them is varied systematically. The results indicate that both these parameters have a profound influence on the flow field. The reattachment points, the wake structure and the flow between the two obstructions change considerably with the variation of these parameters. The study brings out these effects.**

Keywords: Constrictions with sinusoidal geometry, Channel, Tandem arrangement, Interference effects.

INTRODUCTION

Obstructions occur on arterial walls mainly due to deposition of fatty material. Over a period of time these grow and occupy a substantial portion of the arteries. These are called stenotic obstructions and give rise to serious physiological conditions. The growth of the stenosis can be expected to be considerably influenced by the flow phenomena at various degrees of constrictions. There is a possibility of occurrences of another obstacle nearer to a previously formed one. This newly formed obstacle can occur on the same side or opposite side of the previous one. These obstacles can begin and grow simultaneously at the same rate or at different rates over a period of time or they can form one after another. It is essential to understand the flow past such obstructions and the resulting stresses on the lumen. To gain such understanding flow past simplified models of these obstructions with different geometries and varying sizes are made. The present study is one such investigation; semi-circular geometry is made use of and obstructions are considered on the same side of a channel wall. Tandem arrangement is considered. Lakshmana Gowda [1] has considered flow through obstructions in a channel with different degrees of constrictions. He has considered rectangular, semi-circular, sinusoidal and plate geometries in a channel. The obstructions in all cases are located symmetrically at one location. It is reported that the flow field depends both on the degree of constriction and the Reynolds number. Depending on the two parameters mentioned, the flow downstream of the symmetrical constriction could be asymmetrical. However, no interference effects of more than one constriction is reported.

Griffith et. al.[2] have studied two-dimensional flow through a constricted channel. A semi-circular bump is located on one side of the channel and the extent of blockage is varied by adjusting the radius of the bump. The blockage is varied between 0.05 and 0.9 of the channel width and the upstream Reynolds number between 25 and 3000. The geometry presents a simplified blockage specified by a single parameter, serving as a starting point for investigations of other more complex blockage geometries. For blockage ratios in excess of 0.4, the variation of reattachment length with Reynolds number collapses to within approximately 15%, while at lower ratios the behavior differs. For the constrained two-dimensional flow, various phenomena are identified, such as multiple mini recirculations contained within the main recirculation bubble and vortex shedding at higher Reynolds numbers. The stability of the flow to three-dimensional perturbations is analysed, revealing a transition to a three-dimensional state at a critical Reynolds number which decreases with higher blockage ratios. Separation lengths and the onset and structure of three-dimensional instability observed from the geometry of blockage ratio 0.5 resemble results taken from backward-facing step investigations. The question of the underlying mechanism behind the instability being either centrifugal or elliptic in nature and operating within the initial recirculation zone is analytically tested.

Sobey and Drazin [3] have investigated some instabilities and bifurcations of two-dimensional channel flows using analytical, numerical and experimental methods. They start by recapitulating some basic results in linear and nonlinear stability and drawing a connection with bifurcation theory. Then examine Jeffery–Hamel flows and discover new results about the stability of such flows. Next they have considered two-dimensional indented channels and the resulting symmetric and asymmetric flows. It is demonstrated that the unique symmetric flow which exists at small Reynolds number is not stable at larger Reynolds number, there being a pitchfork bifurcation so that two stable asymmetric steady flows occur. At larger Reynolds number it is found as many as eight asymmetric stable steady solutions, and the existence of another seven unstable solutions infered. When the Reynolds number is sufficiently large they find time-periodic solutions and deduce the existence of a Hopf bifurcation. These results show a rich and unexpected structure to solutions of the Navier–Stokes equations at Reynolds numbers of less than a few hundred.

International Journal of Engineering Research & Technology (IJERT)
ISSN: 2278-0181
Vol. 7 Issue 08, August-2018

Mandal and Chakrabarthi [4] have carried out a numerical study for rectangular stenosis with different stenosis length and for degree of constriction 50%. Wall pressure, streamline contour, axial velocity profile, wall shear stress have been studied and their psychological aspect have been discussed. It was reviled that the pressure drop and wall shear stresses are dependent upon the stenosis length. Axial velocity profile and reattachment length are relatively independent of stenosis length. During initiation of stenosis length, the appreciable increase in the peak wall shear is noted, this magnitude of weak wall shear stress is observed to be decreasing with the progression of stenosis length. There is no change in size of recirculation zone, axial velocity profile and low shear stress with stenosis length. Therefore, the chance of tearing action and collapse of endothelium wall increases with the progression of stenosis length, as the wall pressure is thought to be one of the prime causes of this phenomenon. Since recirculation zone is not depending on the stenosis length, therefore it can be stated that during initiation of the stenosis length, maximum possibility of lipid deposition on the wall may take place, but the phenomenon may not take place with further increase in stenosis length. The maximum cell turnover point on the arterial wall due to reattachment point moves downstream with stenosis length. Wall damage and decrease with the progression of stenosis length.

There appears to be very little information on the interference effects of the obstructions when more than one is present on the flow field. In this study, flow past sinusoidal obstructions arranged on the same side of a channel in tandem arrangement with varying relative sizes is investigated. Flow visualization is made use of for the investigation. The configuration considered is shown in Fig.1. The length of the channel is L and the width W. The height (amplitude) of the upstream sinusoidal block is r and the height of the interfering block is r_i. The center to center distance between the obstructions is s.

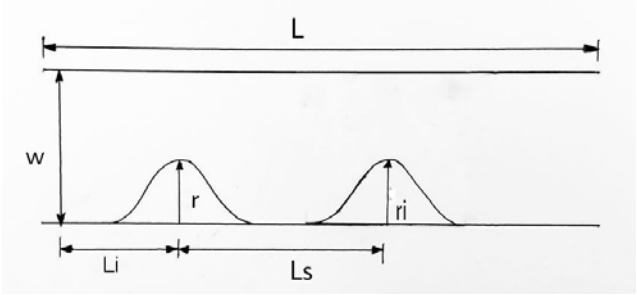

Fig. 1 Configuration considered

EXPERIMENTAL ARRANGEMENT

Experiments have been conducted using Flow Visualization Facility which is available at the fluid mechanics laboratory, Department of Mechanical Engineering, B.T.L. Institute of Technology. This facility consists of a F.R.P tank with 2.5 m length and breadth of 1.5 m (Fig. 2) and a set of aluminum discs, separated by a small distance are located at one end of the tank. The discs are connected to a three phase induction motor with cooling arrangement through a set of bevel gears and the flow created from the rotation of the discs is guided into the test section by two guide blocks made of FRP. The width of this test section is 350mm. By controlling the speed of the motor, the speed in test section could be varied continuously up to 0.2 m/s. At higher speeds the water becomes wavy and hence for the experiments a suitable speed is chosen where such waves do not occur. Fine aluminum powder is used as a tracer medium. Single-Lens Reflex (SLR) camera is be used to photograph the flow field. The camera is placed at a suitable height above the channel containing baffle plates. Two Halogen 500 watts lamps are used to obtain proper lighting.

The sinusoidal models are made out of 2 mm thick mild steel plates and fixed to the sides of a channel 50 mm wide (W). The height (amplitude) of the upstream obstruction (r) and the downstream interfering obstacle (r_i) used are 20 mm, 25 mm, 37.5 mm and 45 mm. The degree of constriction, D, is defined as r/W and the relative constriction ratio is defined as r/r_i. The spacing ratio L_s is defined as s/W where s is the distance between the centers of the two obstructions (Fig.1). The Reynolds number is defined as $2UW/\nu$ where U is mean velocity in the channel and ν is the kinematic viscosity. All the cases considered here have same free stream velocity U = 0.073m/sec and Reynolds number is kept constant as 9125. The experiment is carried out by keeping the upstream obstacle of constant to get r/W = 0.4, 0.5, 0.75 and 0.9. For each r/W the height of the downstream obstacle is varied to get D = 0.4, 0.5, 0.75 and 0.9. For each of this combination, interference length ratio is varied as L_s= 2, 2.5, 3, 4 and 5 and results obtained.

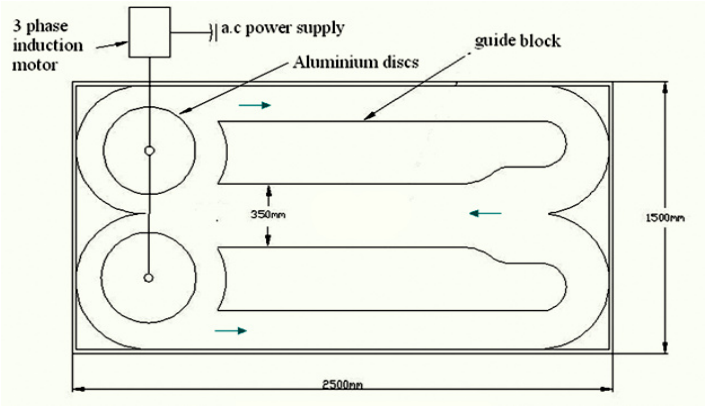

Fig. 2: Experimental arrangement

RESULTS

The results have been obtained for r/w = 0.4, 0.5, 0.75 and 0.9 and for each r/w, r_i/w = 0.4, 0.5, 0.75 and 0.9. However, results with r_i/w = 0.4 are not presented to restrict the number of pages. To obtain a better prospective of the results with interference, results for the case without interference (i.e., single sinusoidal obstruction with different r/w values) is presented first in Fig.3.

From Fig.3, it is seen that the area of the flow decreases as the obstacle is introduced with increasing value of D (degree of constriction) of the obstacles. Flow separation takes place when it passes through the gap between the obstacle and the channel wall due to the adverse pressure gradient occurring

International Journal of Engineering Research & Technology (IJERT)
ISSN: 2278-0181
Vol. 7 Issue 08, August-2018

on the downstream side of the obstacle. The separation takes place at the peak of the obstacle in all cases. At D = 0.4 (Fig.3a), vortex patterns are seen in the wake and also the flow is wavy for sufficient distances downstream. There are also local separation zones on the top side. As the value of D increases (Fig.b,c,d), the waviness in the wake flow disappears. The flow reattachment length behind the obstacle increases up to D = 0.75. However, at D = 0.9, the reattachment length decreases with a distinct change in the wake flow pattern.

When an obstacle is introduced downstream, it will interfere with the wake and changes the flow field behind the front obstacle. The results for r/W = 0.4 and r_i/W = 0.5 for various values of s/W are shown in Fig. 4b to 4f. In Fig. 4b (s/W = 2), a vortical pattern is formed between the two obstacle. There is a streamlining effect due to interference effect. The flow on the downstream obstacle separates beyond the peak and then the reattachment occurs. The wake is very much different from the single obstacle case (Fig.4a). At s/W = 2.5 (Fig.4c), the flow pattern is nearly same as that for s/W = 2 (Fig.4a) except that the recirculation region as increased between the two obstacles. For s/W = 3 (Fig.4d), the reattachment of the flow separating from the front obstacle attaches at the mid face of the downstream obstacle. Vortical flows between the obstacle appear to coalesce. The reattachment length behind the rear obstacle increases. For s/w = 4 (Fig.5e), the flow reattaches behind the front obstacle and also behind the rear obstacle. The reattachment length behind the front obstruction is nearly same as that for the obstruction without interference (Fig.5a). There is slight dip in the jet like gap flow. Similar trends in the flow field are seen in Fig.5f for s/W = 5. When the spacing between the obstacles increases further (s/W = 4, Fig.5e) the reattachment of the flow between the obstacles occurs near the foot of the rear obstacle and a long near wake occurs behind the front obstacle. The wake behind the rear obstacle shortens compared to the earlier cases Fig. 5b to d). At s/W = 5 (Fig.5f), the reattachment of the flow separating from the front obstacle occurs in between the obstacles. The reattachment length behind the downstream obstacle is short.

For r/W = 0.4 and r_i/W = 0.75 (Fig.5) i.e., when the height of the interfering obstacle increases, there is considerable difference in the flow pattern compared to that for the previous case (Fig.4). For s/W = 2 (Fig.5b), there is a vortex hugging the lower front portion of the interfering obstacle. The flow separates from this obstacle downstream of its peak, with a reattachment point on the side of the channel. This pattern changes at s/W = 2.5 both between the obstacles and behind the rear obstacle. The separation point of the flow from the top of the rear obstacle moves towards the peak which results in a larger wake width and reduced reattachment length. At s/W = 3, the reattachment length decreases further. There is not much change in the flow between the obstacles. At s/W = 4, the separating flow from the top of the front obstacle reattaches near the foot of the rear obstacle with a large vortex being formed. The reattachment length behind the rear obstacle is nearly same as for the previous case. With further increase in s/W to 5 (Fig.5e)the reattachment between the obstacles occur close to the front body. This results in a change in the approach flow with respect to the rear body. The flow separation occurs almost at the top and the wake pattern changes.

When the height of the interfering obstruction r_i/W increases to 0.9 (Fig.6), it has very significant effect on the flow field of the upstream obstacle at all values of relative spacing s/W. For s/W = 2, the flow is lifted and attaches on to the downstream obstruction. As the spacing increases, the flow field between the two obstacles change as also the flow behind the interfering obstruction. For spacing above 3, a separation zone on the upper channel wall between the two obstructions is seen (Fig. 6e and f). This is mainly due to the downward movement of the flow on top of the front obstacle. The flow reattachment between the obstacles occur even at s/W = 4 and of course for s/W = 5. Due to this there is a strong surface flow along the front face of the rear obstacles for both these spacing (Fig.6e and f). Strong wall jet flows along the top channel wall are seen for these cases. These changes in the flow field can be expected to have considerable effect on the stresses on the walls of the channel.

The results for the case with r/W = 0.5 and r_i/W = 0.5 at various values of s/W are shown in Fig.7b to 7f. At s/W = 2 (Fig.7b), the interfering obstacle has a streamlining effect and a stationary vortical flow occurs between the obstacles. Flow reattachment behind the rear obstacle occurs. Above the reattachment zone a strong flow is seen. As the spacing between the obstacles increases (Fig.7c and d) the flow between the bodies change as the flow separating from the front obstacle reattaches on different points on the front face of the downstream obstacle. The wake behind the rear obstacle shortens. At s/W = 4 (Fig.7e), the reattachment of the flow separating from the front body occurs almost at the foot of the rear body. This changes the flow around the rear obstacle with a very short near wake behind. When s/W = 5 (Fig.7f), the reattachment occurs in between the bodies and the flow around the rear obstacle is nearly same as that for the no-interference case (Fig.7a).However, the wake is slightly shorter probably due to the increase in the approach turbulence.

When r/W = 0.5 and r_i/W = 0.75 (Fig.8), significant changes occur at s/W = 2, 2.5 and 3. At 2 (Fig.8b) the separating flow from the front body hits the peak of the rear body and the flow is deflected up. With the result a very large wake is formed with no clear reattachment point being seen. At 2.5 (Fig.8c) the flow from the top of the rear obstacle bends and still no clear reattachment point seen. At 3 (Fig.8c) continues with flow reattaching at sufficiently long distance behind the rear body. From s/W = 2, 2.5 and 3 the separating flow from the peak of the front body attaches on to the front face of the rear body at continuously decreasing distances from the peak. This has an effect both on the recirculating flow between the bodies and the flow on the front face of the rear body (Fig.8b,c and d). At s/W = 4 (Fig.8e), the reattachment of the flow between the bodies occur close to the foot of the body with a clear wake behind the front obstacle. There is flow along the front face of the rear body and a wake with reattachment point is seen. When the spacing is further increased (Fig.8f), both the bodies act as individual

International Journal of Engineering Research & Technology (IJERT)
ISSN: 2278-0181
Vol. 7 Issue 08, August-2018

obstacles. However, there are interference effects affecting the wake of both the obstacles.

Figure 9 shows the results for r/W = 0.5 and r_i/W = 0.9 for various values of s/W. As can be seen the interfering obstacle has a significant effect on the flow behind the front obstacle. The vortical flow between the bodies change considerably as the spacing changes. Even at s/W = 3, the reattachment of the flow separating from the front body occurs in between the two bodies. This results in a change in the flow on the front face of the rear body. As s/W increases to 4 and 5, the flow between the cylinders change with two vortical pattern seen at s/W = 5. Behind the rear obstacle a wall jet like flow occurs at all spacing with the wake extending for long distance downstream.

Figure 10 shows the results for r/W = 0.75 and r_i/W = 0.5 for different spacing. The result at Fig.10a is for the single obstacle. It is seen that for s/W = 2, 2.5 and 3 (Figs.10b,c and d), the interfering obstacle affects the wake behind the front obstacle. There is a trapped vortex between the bodies in all these cases which grows in size as the spacing increases. The rear body appears to be within the wake of the front body. Reattachment behind the rear obstacle occurs. At s/W = 4, the flow separating from the front obstacle attachés on the front face of the rear body. This point of attachment moves down almost to the foot of the face at s/W = 5 (Fig.10f). Due to this there is vortical flow with number of vortices between the bodies. There is corresponding change in the wake behind the rear body with a slightly enlarged near wake.

For r/W = 0.75 and r_i/W = 0.75 (Fig.11), a strong jet-like gap flow occurs between the obstacles adjacent to the top wall, the two obstructions acting like a compound body. At s/W = 2 and 2.5, there are stationery vortices between the bodies. As the spacing increases to 3, more than one vortex is seen between the obstructions. At s/W = 4 the flow from top of the front body bends to reattach mid face of the rear body. At s/W = 5, reattachment occurs between the bodies and a complex system of vortices is seen. There is flow on the front face of the rear body.

At r_i/W = 0.9 (Fig.12), due to the increased height and width of the interfering obstruction, the gap flow persists for long distances behind the downstream body with a complex system of vortical flow and a nearly dead water region. The rear body causes a streamlining effect and there is a stagnant vortex between the bodies which increases in size as the spacing increases (Fig.12b,c and d). At s/W = 4, there is reattachment in the gap between the obstructions almost at the base of the rear body. As spacing increases to s/W = 5, the reattachment point occurs at about three fourths the distance between the bodies. Due to this there is a strong flow along the front face of the rear body.

The results for r/W = 0.9 and r_i/W = 0.5, 0.75 and 0.9 at various spacing are shown in Figs. 13, 14 and 15 respectively. In all the cases, there is a strong wall jet like flow issuing from the top of the front obstacle. For s/W = 2, 2.5 and 3, there is a trapped vortex between the two obstacles whose size increases with the spacing. As the height of the interfering obstacle increases (i.e., s/W = 0.5, 0.75 and 0.9) the flow separating from the front obstacle bends and attaches on to the front face of the rear obstacle. This feature occurs for s/W = 4 and 5 also in a more marked manner. More than one vortical pattern is seen between the bodies. However, even at these larger spacing there is no flow reattachment between the bodies.

CONCLUDING REMARKS

Flow visualization results when two obstructions with sinusoidal geometry have been presented. The obstructions are placed in tandem arrangement and the spacing between them varied systematically. The effect of the change in relative size of the obstructions is investigated.

The results indicate that the geometry, relative size and spacing have a profound effect on the flow field. When the two obstacles are close there is invariably stationery vortex flow between them. The shape and orientation of this trapped vortex is influenced by the shape of the obstacle. If the upstream obstacle is relatively smaller than the downstream obstacle, there is a upward swing in the flow between the obstacles. In the vice versa case, the downstream obstacle is submerged in the wake of the upstream obstruction. When the constrictions are severe, invariably there is a wall jet like flow on the channel side opposite to the obstacles which persists for long downstream distances. The reattachment of the flow between the bodies is decided by the geometry, spacing and the relative sizes. For relatively smaller size of the front obstruction used, the reattachment occurs for relative spacing larger than 4. The wake behind the downstream obstruction is altered considerably with a large number of vortices. However, no regular vortex shedding is seen.

The changes in the flow field seen with interference effect has considerable effect on the stresses created on the channel walls. Such situations occur around obstructions/stenoses created in an artery. The present study helps to understand the flow field changes that could occur in real situations.

ACKNOWLEDGEMENTS

The authors express their sincere thanks to the management of BTL IT for their support and encouragement.

REFERENCES

[1] B. H. Lakshmana Gowda. A Kaleidoscopic View of Fluid Flow Phenomena, Published by Wiley Eastern Limited (1992).

[2] M. D. Griffith, M. C. Thompson, T. Leweke, K. Hourigan and W. P. Anderson. Wake Behaviour and Instability of Flow through a Partially Blocked Channel. J. Fluid Mech. (2007), vol. 582, pp. 319–340.

[3] an J. Sobey and Philip G. Drazin, Bifurcations of two-dimensional channel flows, J. of Fluid Mmechanics, vol. 171, pp. 263-387.

[4] D. K. Mandal and S. Chakrabarti, Effect of Stenosis Length on Flow Characteristics Across Rectangular Stenotic Models, International J. of Fluid Mechanics, vol. 5(1) (2013); pp. 29-39.

NOMENCLATURE

L = length of the channel
W = Width of the channel
s = distance between the centre of the obstacles
r = height of the upstream sinusoidal obstacle

International Journal of Engineering Research & Technology (IJERT)
ISSN: 2278-0181
Vol. 7 Issue 08, August-2018

r_i = height of the downstream sinusoidal obstacle
Degree of constriction D = r/W
Relative spacing ratio: s/W

(a)0.4

(b)0.5

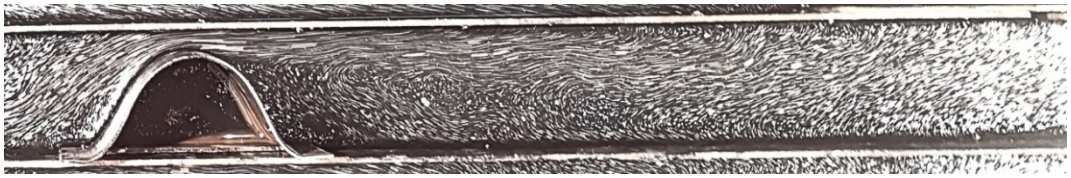

(c)0.75

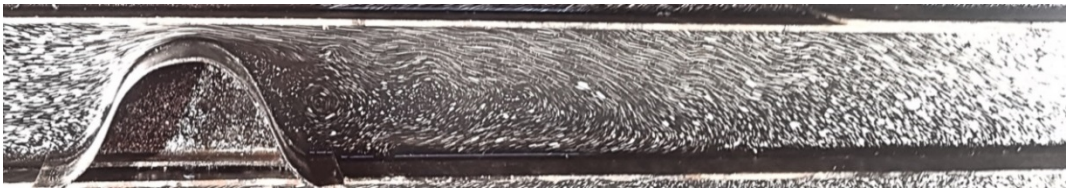

(d)0.9

Fig.3 Flow field for single obstacle, for various Degree of Constriction (D)

s/W

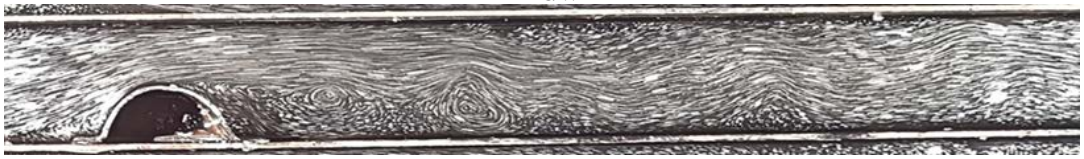

(a)

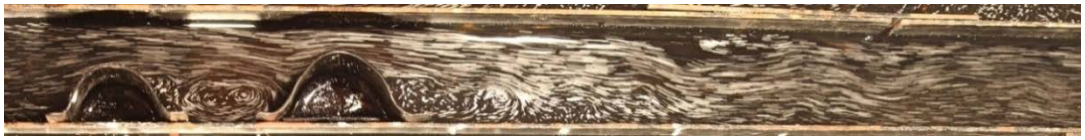

(b) 2

(c) 2.5

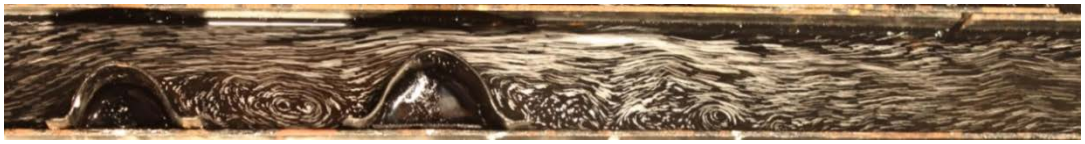

(d) 3

International Journal of Engineering Research & Technology (IJERT)
ISSN: 2278-0181
Vol. 7 Issue 08, August-2018

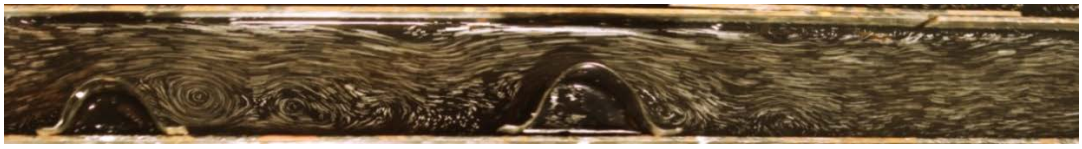

(e) 4

(f)5

Fig.4 Flow pattern for r/W=0.4, r_i/W=0.5, for various s/W ratio.

s/W

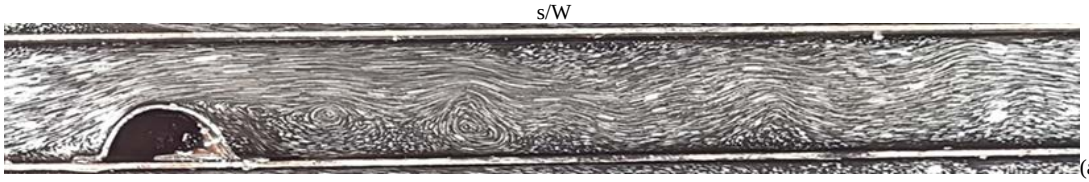

(a)

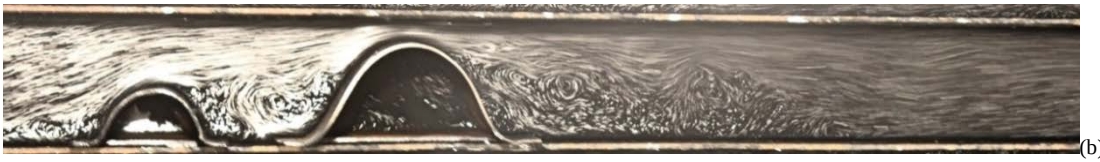

(b) 2

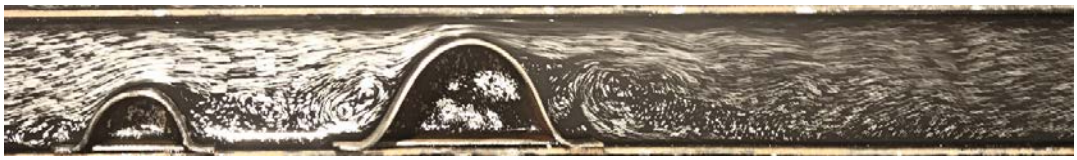

(c) 2.5

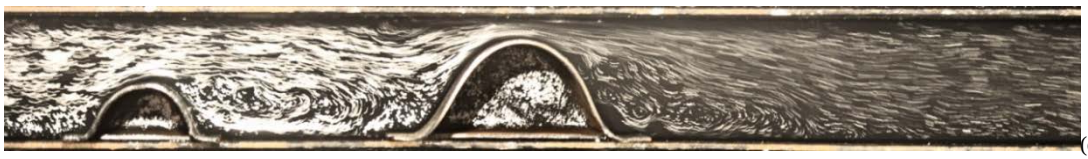

(d)3

(e) 4

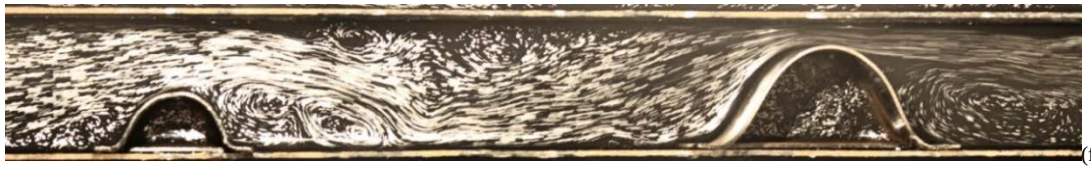

(f) 5

Fig.5 Flow pattern for r/W=0.4, r_i/W=0.75, for various s/W ratio.

International Journal of Engineering Research & Technology (IJERT)
ISSN: 2278-0181
Vol. 7 Issue 08, August-2018

s/W

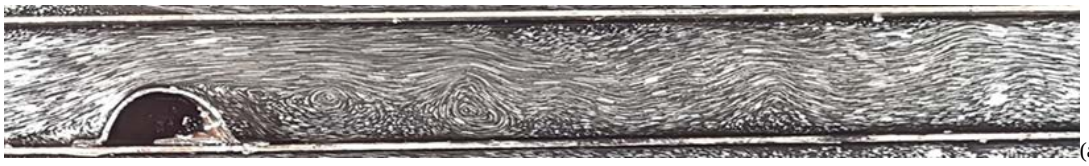
(a)


(b)2

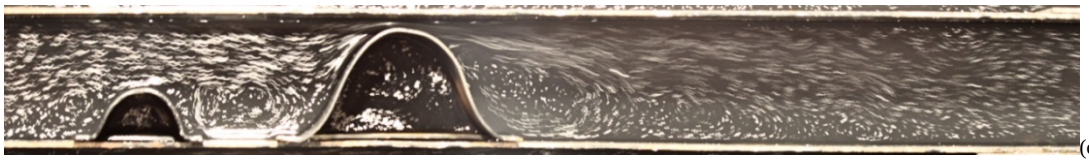
(c)2.5

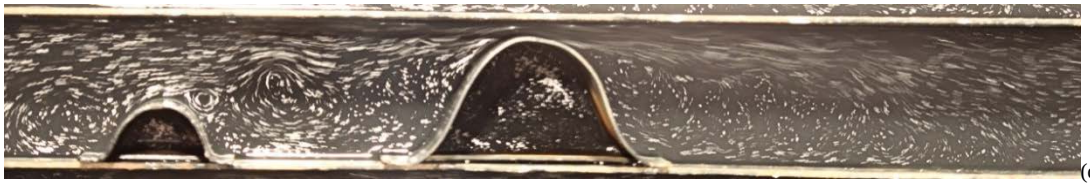
(d)3

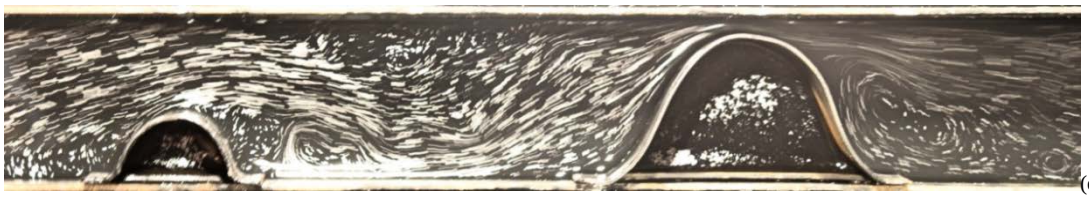
(e)4

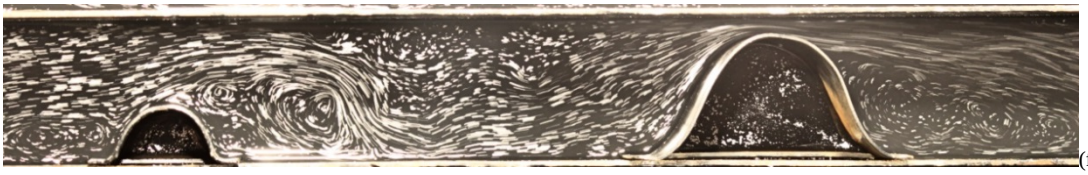
(f)5

Fig.6 Flow pattern for r/W=0.4, r_i/W=0.9, for various s/W ratio.

s/W

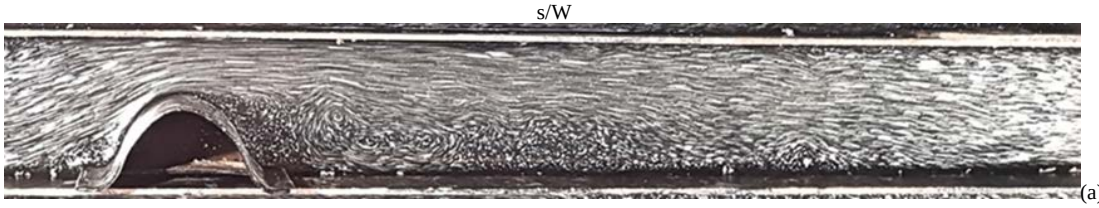
(a)

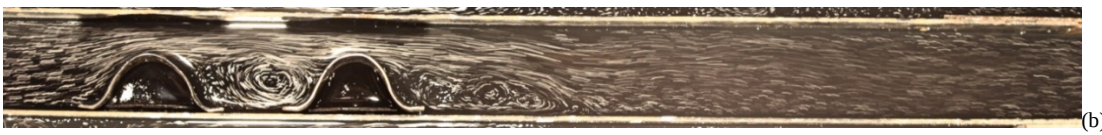
(b) 2

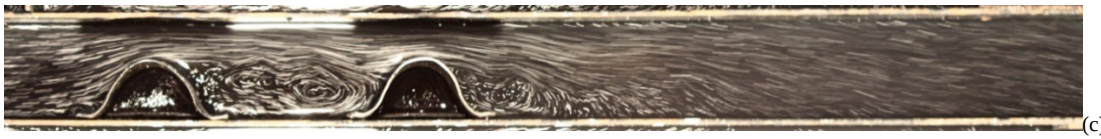
(c) 2.5

International Journal of Engineering Research & Technology (IJERT)
ISSN: 2278-0181
Vol. 7 Issue 08, August-2018

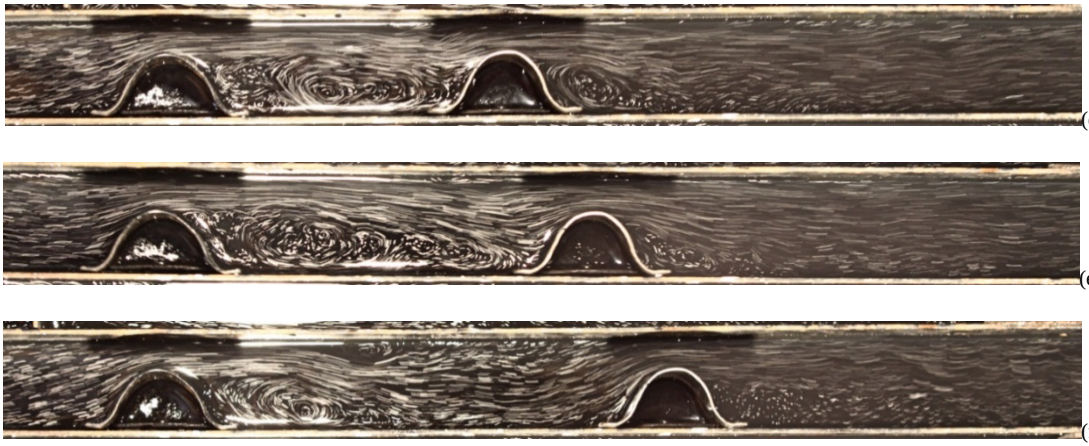

Fig.7 Flow pattern for r/W=0.5, r_i/W=0.5, for various s/W ratio.

Fig.8 Flow pattern for r/W=0.5, r_i/W=0.75, for various s/W ratio.

International Journal of Engineering Research & Technology (IJERT)
ISSN: 2278-0181
Vol. 7 Issue 08, August-2018

Fig.9 Flow pattern for r/W=0.5, r_i/W=0.9, for various s/W ratio.

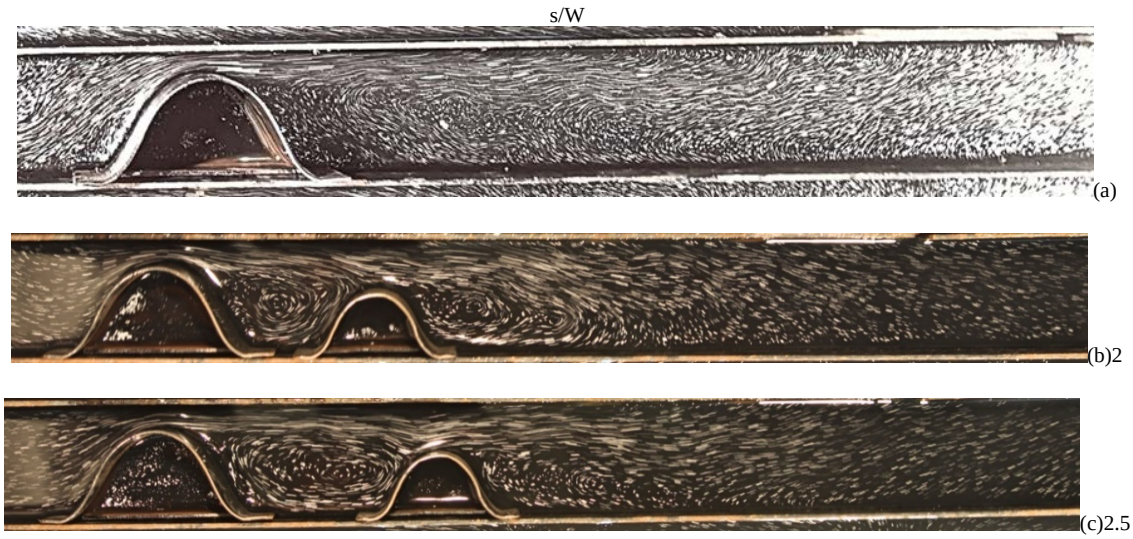

International Journal of Engineering Research & Technology (IJERT)
ISSN: 2278-0181
Vol. 7 Issue 08, August-2018

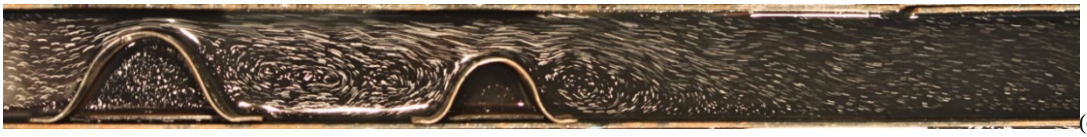

(d)3

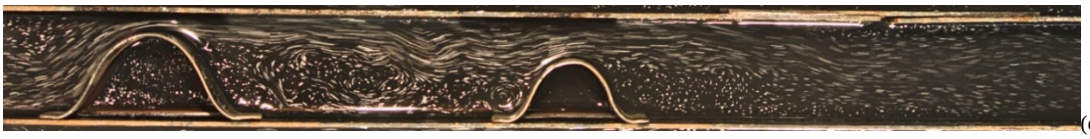

(e)4

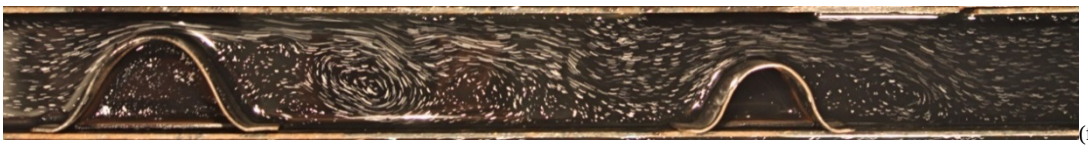

(f)5

Fig.10 Flow pattern for r/W=0.75, r_i/W=0.5, for various s/W ratio.

s/W

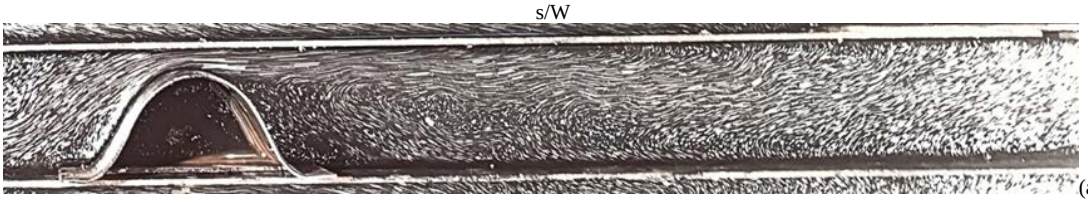

(a)

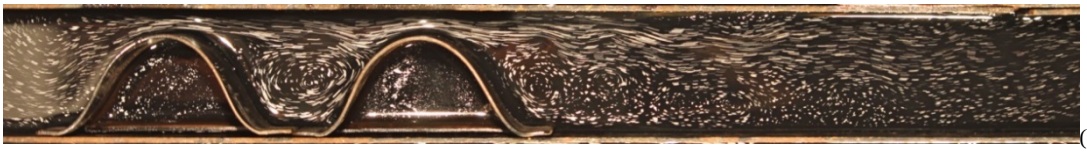

(b)2

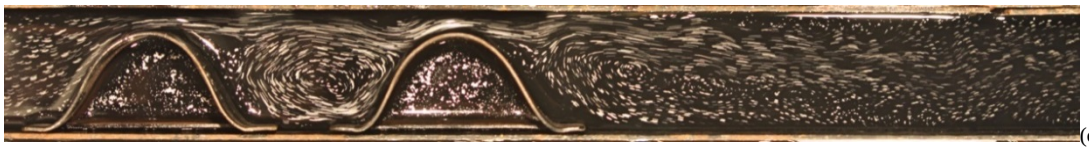

(c)2.5

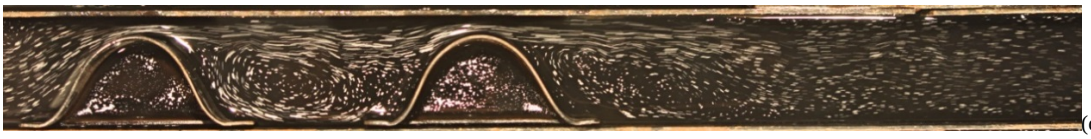

(d)3

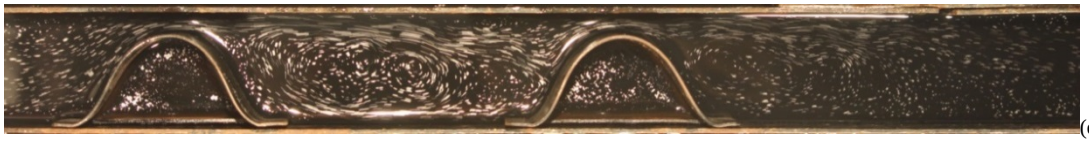

(e)4

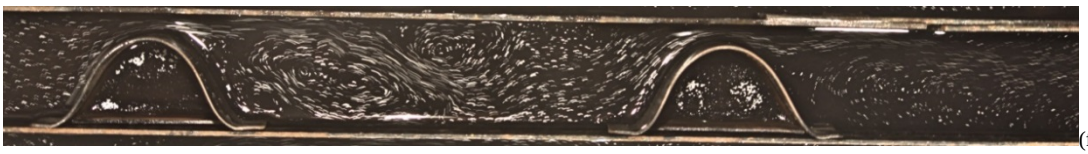

(f)5

Fig.11 Flow pattern for r/W=0.75, r_i/W=0.75, for various s/W ratio.

s/W

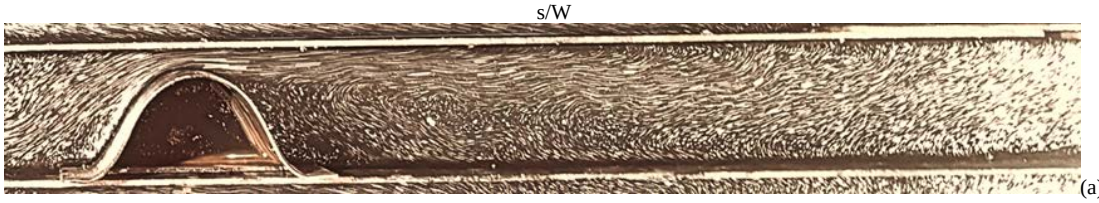

(a)

International Journal of Engineering Research & Technology (IJERT)
ISSN: 2278-0181
Vol. 7 Issue 08, August-2018

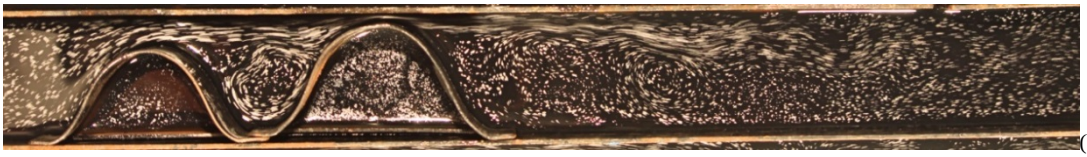

(b)2

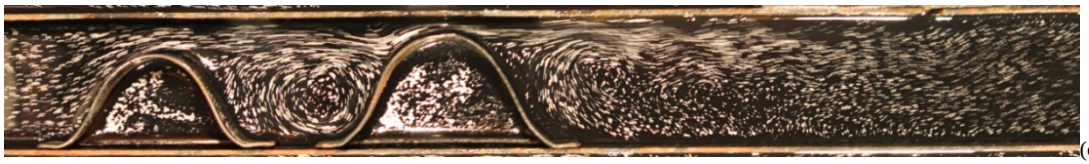

(c)2.5

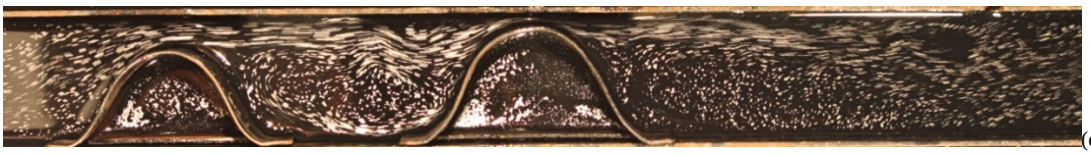

(d)3

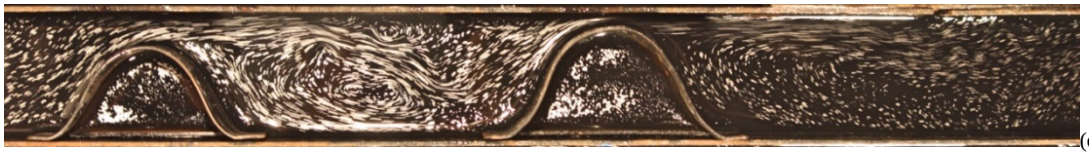

(e)4

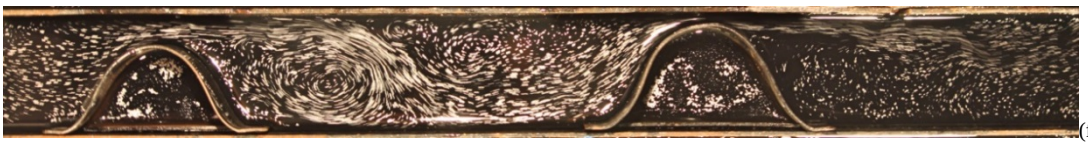

(f)5

Fig.12 Flow pattern for r/W=0.75, r_i/W=0.9, for various s/W ratio.

s/W

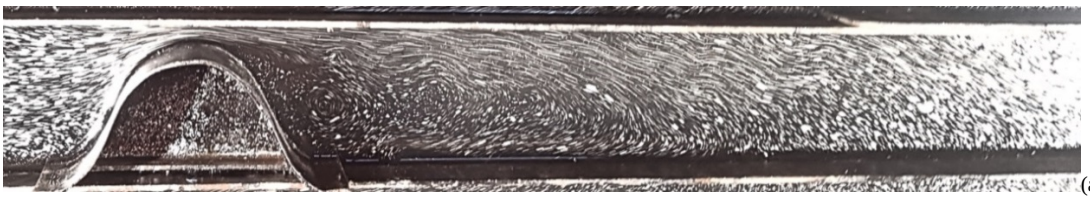

(a)

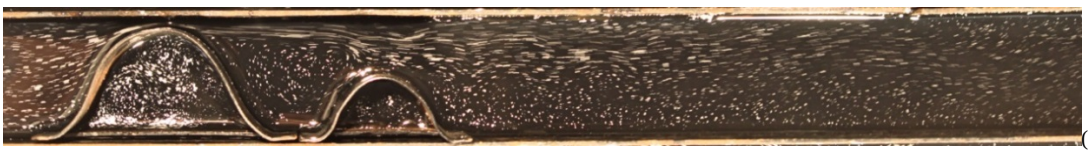

(b)2

(c)2.5

(d)3

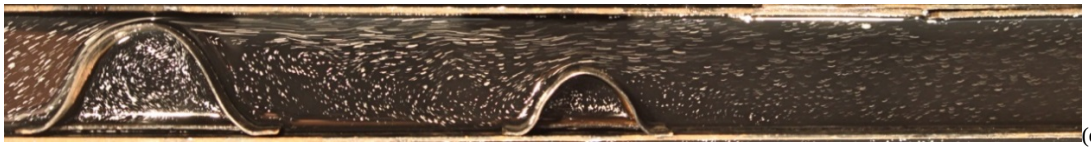

(e)4

International Journal of Engineering Research & Technology (IJERT)
ISSN: 2278-0181
Vol. 7 Issue 08, August-2018

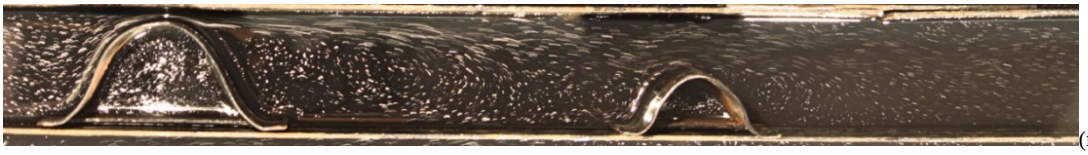

(f)5

Fig.13 Flow pattern for r/W=0.9, r_i/W=0.5, for various s/W ratio.

s/W

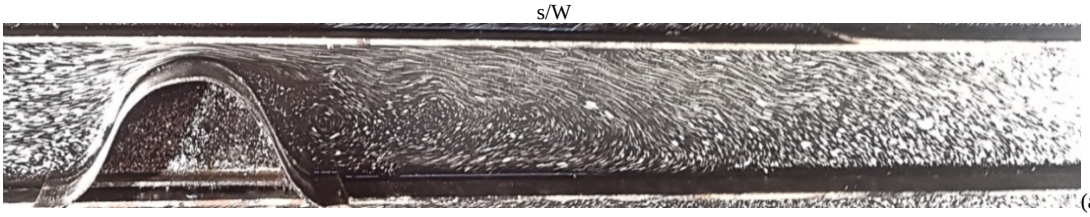

(a)

(b)2

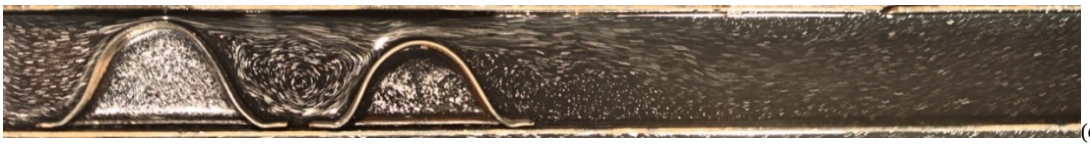

(c)2.5

(d)3

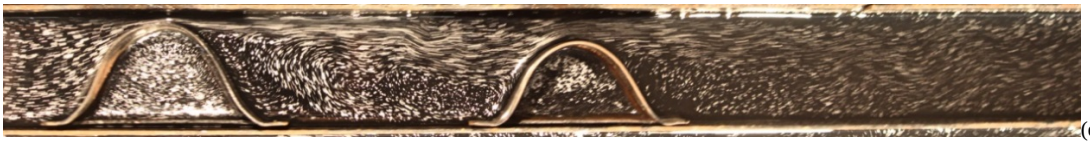

(e)4

(f)5

Fig.14 Flow pattern for r/W=0.9, r_i/W=0.75, for various s/W ratio.

s/W

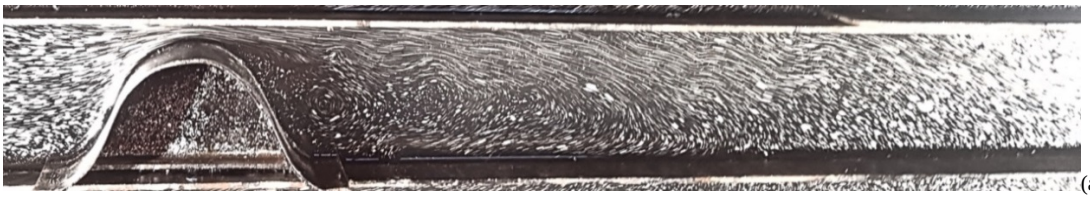

(a)

(b)2.3

International Journal of Engineering Research & Technology (IJERT)
ISSN: 2278-0181
Vol. 7 Issue 08, August-2018


(c)2.5

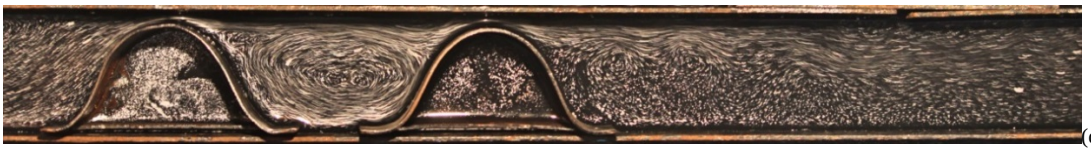
(d)3

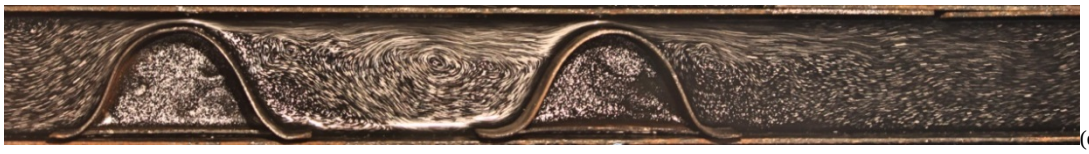
(e)4

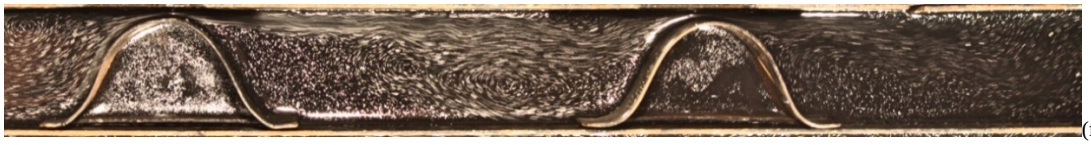
(f)5

Fig 15: Flow pattern for r/W=0.9, r_i/W=0.9, for various s/W ratio.